International Journal of
AI ELECTRICAL CIVIL AND MECHANICAL ENGINEERING
Peer Reviewed, Referred & Indexed Journal
ISSN: 3070-0434 www.zesterapublications.com Original Research Paper

ELECTRIC VEHICLE-TO-VEHICLE (V2V) ENERGY TRANSFER USING MOTOR INVERTER AND WINDING

Naresh Jella
Assistant Professor
Dept of EEE
St Peter's Engineering College,
Hyderabad
nareshjella@stpetershyd.com

N GANESH
Dept of EEE
St Peter's Engineering College,
Hyderabad
Nganeshnayak555@gmail.com

Abstract—***Among the most effective methods for lowering automobile emissions is the electrification of automobiles. People are hesitant to promote electric cars (EVs) due to concerns about their range. By addressing the "last mile" issue, energy transfer between EVs helps reduce range anxiety in an emergency. Nevertheless, optimising efficiency is not taken into account by the current vehicle-to-vehicle (V2V) energy-sharing technique, which relies on motor inverters and motor windings. A novel V2V architecture is suggested to solve this problem by utilising a control mechanism involving soft-switching and a decreased switching frequency. When transferring power from a voltage source to a motor with an inductor winding and core made of silicon steel, a reduced switching frequency can significantly cut down on core loss. Simulation results at 150 kW and laboratory scale-down power tests at 1.5 kW prove the efficacy of the suggested strategy. This research presents a novel vehicle-to-vehicle (V2V) energy transfer technique that utilises the inverters and windings of two electric vehicles to address these issues.***

The suggested technique makes advantage of three-phase interleaved control, which enables the effective and smooth sharing of power between two vehicles. The control system modifies the duty cycle and switching frequency in response to the needed power level and the voltages of the batteries. The system becomes adaptable and can handle various charging situations because of this.
The concept was validated through the use of 150 kW simulation testing and 1.5 kW laboratory studies. The outcomes demonstrate that the system is functioning as intended, achieving extremely high efficiency while maintaining a motor torque close to zero. About 99.47% efficiency was the highest value measured.

In conclusion, this study lays forth a straightforward, inexpensive, and very effective method of V2V charging that makes use of already electric vehicle parts. Reduced energy loss and improved reliability are the results of the suggested method's use of soft-switching control and low switching frequency operation. This method can alleviate concerns about EV range and make them more useful in times of urgency when charging is not an option.

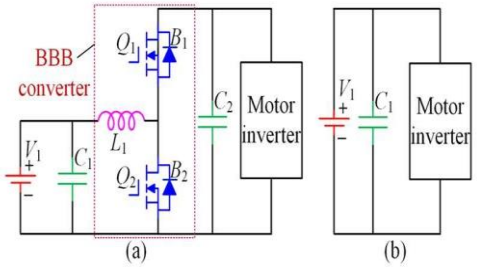
Keywords— Electric vehicle (EV), battery charging, dc rapid charging, zero voltage switching (ZVS), vehicle-to-vehicle (V2V), and soft-switching were all used.

I INTRODUCTION

To reach carbon neutrality, it is possible to combine the electrification of transportation with the development of additional energy power [1]. Range anxiety and a lack of charging infrastructure, however, are preventing EVs from being widely used [2]. The use of vehicle-to-vehicle (V2V) charging, in which a high energy EV charges a low-energy EV, can help with range anxiety and the limits caused by inadequate charging infrastructure in emergency situations [3]. There are now three main types of vehicle-to-vehicle energy sharing systems [4]. Connecting two electric vehicles to a single external, or off-board, charger is the first type. For example, in order to facilitate energy transmission between cars, a single-phase bridgeless converter is suggested as an off-board charger in [5]. A bidirectional buck-boost (BBB) converter coupled with an external charger is recommended by Ucer et al. [6] for V2V energy transfer. V2V power transmission applications can also make use of dc/dc converters as off-board chargers, such as the CLLC converter [8] or the dual active

International Journal of
AI ELECTRICAL CIVIL AND MECHANICAL ENGINEERING
Peer Reviewed, Referred & Indexed Journal
ISSN: 3070-0434 www.zesterapublications.com Original Research Paper

bridge converter [7]. Further, a 75 kW commercial electric vehicle (EV) mobile charging station is planned for use in [9]. The main issue with off-board V2V chargers, meanwhile, is the additional expense, weight, and space they demand from customers. The second approach includes some bidirectional on-board chargers (OBCs) that are able to accomplish V2V power-sharing. As mentioned in references [10], [11], and [12], power is transferred using the onboard charger's single-phase inverter. But most OBCs consist of an inverter and an isolation dc/dc converter. This lowers the power conversion stage and
improves power efficiency, allowing the two EVs to be linked through the two-isolation dc/dc converters without an inverter [13]. The cost is reduced in [14], [15], and [16] by replacing the isolation dc/dc converter with a non-isolation BBB converter. In an emergency, V2V power sharing might be rather lengthy, since it takes around 1 hour to charge 10% of a 74-kWh battery with a 7.4 kW OBC, which is the normal maximum power of OBCs [17]. V2V power transmission may be accomplished by wireless charging in vehicles. The idea of vehicle-to-vehicle wireless power transfer (V2V WPT) is proposed as a solution to the problems of limited public charging infrastructure and range anxiety in [18]. By monitoring and comparing the voltage and state of charge (SoC) of electric cars, even while they are in motion, with a wireless charging system, EV owners may switch between charging and discharging their vehicles [19]. Nevertheless, there is currently no viable and established solution to the limitations imposed by distance and the placement of the induction coil on the wireless charging systems suggested in [18] and [19]. It is also important to fix the issue of wireless charging induction coil misalignment, as it significantly lowers power efficiency [20]. The third approach involves sharing energy via a converter linked to a battery. Two common kinds of converters are depicted in Fig. 1 and are linked to the electric vehicle battery. An electric vehicle's Type I system involves connecting the motor inverter to the battery pack using a BBB converter. In a type II electric vehicle, the motor inverter is connected directly to the battery. The BBB converters of two EVs are linked in [21] using an additional capacitor. An additional capacitor, along with the inductor and lower switch of two BBB converters, creates a bidirectional dc/dc converter that can share power from two different voltage sources. The EV circuit becomes more complicated and expensive with the additional capacitor. Another drawback is that the approach can only transfer power up to a certain point because it uses just two switches.



Here are two common kinds of converters that are linked to the battery of an electric vehicle (Fig. 1). (a) Type I: Converter with BBBB and motor inverter. (b) Motor inverter of Type II.

To address this issue, a novel control approach that relies on a Type I converter was documented in [22]. That is, a buck boost converter is formed by the remaining switches and diodes in the motor inverter and motor winding, with the upper switch of the BBB converter always turned on. The solution suggested in [22] uses additional switches in parallel to decrease power losses when supplying the same amount of power, as opposed to relying solely on a BBB converter in [14]. When factoring in the price of the BBB converter's additional high-current inductor and switches, it becomes clear that the type I converter for the EV battery is not the best option. The type II converter in the electric vehicle's battery determines whether the motor inverter is a three-phase rectifier or three inductors that connect to the three-phase grid for power transmission [23], [24], [25]. In this setup, one set of electric vehicle motor windings and inverters forms a three-phase inverter, while the other set of windings and inverters functions as a rectifier. It is possible to transmit power from V2V in this situation. But torque will be produced since the motor is powered by a three-phase sinusoidal ac current. To convert the motor into an inductor, an extra mechanical lock is required. A dc/dc converter is realised by reconnecting the motor winding between the motor inverter's arms in order to prevent torque generation [26]. Its main drawback is the number of extra mechanical or (electrical) switches needed to change the circuit's configuration. Also, this method's power efficiency is reduced since there are two stages

International Journal of
AI ELECTRICAL CIVIL AND MECHANICAL ENGINEERING
Peer Reviewed, Referred & Indexed Journal
ISSN: 3070-0434 www.zesterapublications.com Original Research Paper

of power conversion. Not only that, but the topology suggested in [27] is also devoid of torque. V2V power transmission, however, requires an additional half-bridge. In addition, the approaches presented in [22] and [26] utilise motor winding as an inductor with a rather high switching frequency (20 kHz in [22] and 15 kHz in [26]), ignoring the fact that silicon steel, the material often used for motor stators, typically has a maximum working frequency lower than 10 kHz [28]. Power transfer efficiency will plummet due to the high frequency's impact on core losses. In conclusion, when it comes to V2V power-sharing applications, the type II converter (Fig. 1) of EV batteries is the way to go. However, it has not been adequately evaluated or used in the current publications to improve transmission efficiency. A V2V architecture that use the type II converter is suggested as a solution to this problem. Keep in mind that the suggested architecture consists of a single power conversion step. Moreover, supplementary parts are unnecessary for the suggested topology. In order to significantly decrease the stator core loss and switching loss, a torque-free control mechanism utilising zero voltage-switching (ZVS) and a reduced switching frequency is suggested, building on the proposed V2V topology.

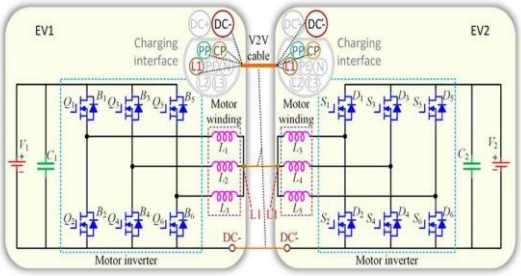


Fig. 2. Proposed V2V topology.

II PROPOSED V2V TOPOLOGY AND OPERATION PRINCIPLE

A. Proposed V2V Topology

Figure 2 depicts the suggested V2V architecture that makes use of the inverter and motor winding of the electric vehicle motor. A V2V cable is used to link the two electric vehicles' charging interfaces. Wherein the L1 and L′1 ports are used to link the neutral points of the motor three-phase windings of the two electric vehicles. Another thing that is linked are the two negative ports (dc-) of the charging interface of the two electric vehicles. A V2V power sharing function may be accomplished using the suggested architecture, which eliminates the need for additional mechanical switches and circuit modifications. The charging interface's PP and CP ports link the communication lines of two vehicles. Realisation of V2V communication and mode selection for V2V charging is possible after appropriate code creation. The design of the Type I converter can also make use of the topology. In the Type I converter, as in [22], the top switch of the BBB converter stays on all the time, and the bottom switch does the same. In such a setup, the electric vehicle's battery and motor inverter are separated by a CLC filter. The peripheral battery circuit has no effect on the functioning of the electric vehicle motor inverter and winding, which are the primary targets of the suggested control approach and topology. Based on this, the topology is likewise applicable to the Type I converter design. Since the suggested V2V architecture depends on the motor inverter and motor winding, it will not be compatible with all EV models. Although the motor inverter is a common part of all electric vehicles, one major drawback is that the neutral point of the motor winding must be easily accessible from the outside. Because of this, you'll need an extra cable to go from the car's body to the charging port. Therefore, the motor and charging system design of the vehicle determines the possibility of using this topology. When two vehicles have differing peak powers, the suggested V2V architecture limits the maximum transfer power to the lowest power ratings of the two vehicles. Keep in mind that there is a certain voltage range for electric vehicle batteries. An 18650-lithium battery, for instance, has a low threshold voltage of 2.75 V and a high threshold voltage of 4.2 V [29]. It is possible for a 400 V EV's battery voltage to drop as low as 275 V. This research takes into account both theoretical and practical possibilities for vehicle-to-grid energy sharing, supposing a battery voltage of 400 V for the high-energy EV and 275 V for the low energy EV. This stipulation served as the basis for all further investigations. Due to significant energy losses at high frequencies, the efficiency of the motor core— made of silicon steel—is reduced, and heat is generated as an undesirable byproduct. Furthermore, certain techniques can cause motor torque, which is the inherently dangerous and inefficient attempt by the motor to spin while charging.

International Journal of
AI ELECTRICAL CIVIL AND MECHANICAL ENGINEERING
Peer Reviewed, Referred & Indexed Journal
ISSN: 3070-0434 www.zesterapublications.com Original Research Paper

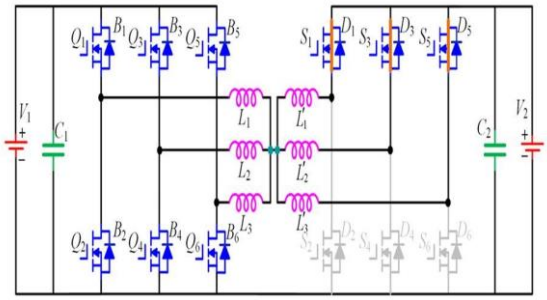


Figure 3. Circuit utilising the suggested way of control. When V1>V2, it means that the power is moving from the left side to the right. While the left-side inverter is operated using the interleaved approach, switches S1, S3, and S5 stay continually ON.

B. Voltage Gain Derivation

The suggested architecture employs a three-phase interleaved parallel control technique to lessen conduction losses via enabling more switches to conduct power in parallel. Here, one motor inverter is controlled by three-phase interleaved operation, while another motor inverter has one set of switches that are always ON.

In Figure 3, we can see the corresponding circuit driven by the suggested control mechanism. In buck mode, left-to-right power flow occurs when V_1>V_2. Here, the left-side inverter is controlled by interleaved modulation, and switches S_1, S_3, and S_5 stay on. Switching to boost mode is as simple as inverting the circuit. When V_1

We take into account the corresponding circuit in Fig.

4 to simplify the voltage gain analysis, where

Leq′=L1′‖L2′‖L3′

It stands for the motor winding's equivalent inductance.

According to the simulation findings, the current via L_eq^'is equal to the total current through L_1, L_2, and L_3. And because it is controlled in three phases interleaved, the current frequency of L_eq^' is three times higher than that of each inductor separately.

Applying the volt-second balance principle to the inductor L_eq^' allows one to determine the voltage gain.

We say that the voltage at three times the switching frequency is

$$v = \frac{v + v + v}{3} \quad (1)$$

wherevan,vbn, andvcn isnodevoltage(asshowninFig.4).

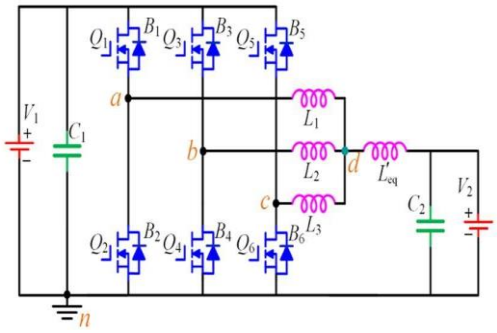


Fig. 4. Simplified equivalent circuit with the proposed control method. Wherein,

L′ eq=L′ 1//L′ 2//L′ 3. And, van, vbn, vcn, and vdn are node voltage produced according to the label in this figure.

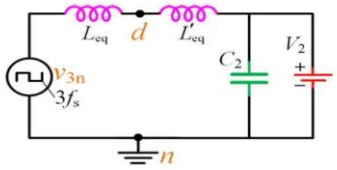


Fig. 5. Further simplified equivalent circuit for calculating three times the switching frequency voltage v3n. where v , v , and v are the node voltages.

The voltage across inductor L is

$$v = \frac{(v - V)L}{L + L} \quad (2)$$

Assuming

Leq′=Leq

Equation (2) becomes

$$v = \frac{v - V}{2} \quad (3)$$

From the inductor voltage waveform, the time intervals t and t are

$$t = \left(d - \frac{2}{3}\right)T$$

$$t = (1 - d)T \quad (4)$$

International Journal of
AI ELECTRICAL CIVIL AND MECHANICAL ENGINEERING
Peer Reviewed, Referred & Indexed Journal
ISSN: 3070-0434 www.zesterapublications.com Original Research Paper

The corresponding inductor voltages are

$$v_{,} = \frac{V - V}{2}$$

$$v_{,t2} = \frac{2V/3 - V}{2} \quad (5)$$

Applying the volt–second balance principle:

$$v_{,}\, t + v_{,}\, t = 0$$

which gives the voltage gain in buck mode as

$$m = \frac{V}{V} = d \quad (6)$$

For boost mode operation, the voltage gain is

$$m_{bo} = \frac{1}{d} \quad (7)$$

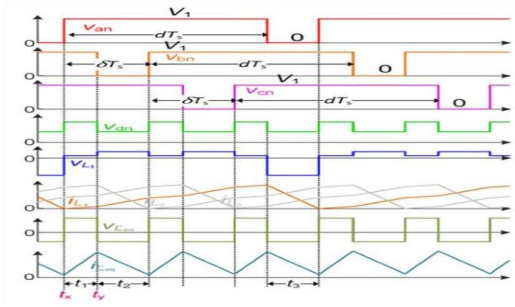


Fig. 6. Waveforms of the inductor voltage and current of interleaved control. Here, phase shift ratio δ = 1/3.

C. Analysis for Zero Torque

The absence of torque production by the motor is the fundamental condition for a control method to be applicable in this topology. The quickest way to accomplish this goal is to ensure that the inductor current is never zero. There is no rotating torque in the motor stator core when there is simply a dc magnetic field.

Inductor L′ eq's ripple current is less than inductor L1's (or L2's, or L3) under three-phase interleaved control. For starters, the current through an inductor L1 (or L2, or L3) is only one half of the frequency of an inductor L′ eq ripple, which is three times higher. So, L′ eq's minimum current will always be larger than zero if and only if L1's minimum current (or L2's, and L3) is greater than zero.

The voltage across an inductor is a good indicator of its current. The voltages across L_1, L_2, and L_3 may be determined using Kirchhoff's Voltage Law (KVL) when the voltage across L_eq^'is known. The three inductors' voltages are indicated by the data in Figure

4.

$$v = v - v$$

$$v = v - v \;,\; v = v - v \quad (8)$$

where

$$v = v - v \quad (9)$$

The current through the inductor $L1$ is used as an example in this examination. The current through the load determines the lowest possible inductor current. By finding the highest and lowest inductor current values, one may represent the load current as

$$\frac{i_{,} + i_{,}}{2} = \frac{I}{3} \quad (10)$$

where I is the output current.

Assuming the minimum inductor current is zero, we can get the critical operating condition by

$$i_{,} = 0$$

In this case, the maximum current via the inductor may be expressed as

$$i_{,} = \frac{v_{,}\, t}{L} \quad (11)$$

where the inductor voltage at time interval t_3 is denoted by v_(L1,t3).

In this case, v_(L1,t3) and t_3 are

$$v_{,} = -\frac{1}{6}(2V + 3V) \quad (12)$$

$$t = (1 - d)T \quad (13)$$

Substituting (6), (12), and (13) into (11), the maximum inductor current becomes

$$i_{,} = \frac{(V - V)(2V + 3V)}{} \quad (14)$$

International Journal of
AI ELECTRICAL CIVIL AND MECHANICAL ENGINEERING
Peer Reviewed, Referred & Indexed Journal
ISSN: 3070-0434 www.zesterapublications.com Original Research Paper

$$6V\,L\,f$$

where $f = 1/T$ is the switching frequency.

When i , = 0, equation (10) can be rewritten as

$$I = \frac{3}{2} i \quad , \qquad (15)$$

The output power can then be expressed as

$$P = \frac{3}{2} V i \quad ,$$

Substituting (14) into the above expression yields

$$P = \frac{V\,(V - V\,)(2V + 3V\,)}{4V\,L\,f} \qquad (16)$$

The output power is regulated by the switching frequency when $V1$, $V2$, and $L1$ are fixed, as is evident from (16). A higher output power is achieved with a lower switching frequency.

Changes in the battery charge cause $X1$ and $V2$ to fluctuate. The available output power drops sharply when $X1$ gets closer to $S2$. The output power is zeroed out when $X1$=$V2$, as shown in equation (16).

In order to examine this impact, we will suppose that the battery voltages change as

$$V = 400 - t$$
$$V = 275 + t \quad , \qquad V - V = 125 - 2t \qquad (17)$$

By plugging (17) into (16), we can get the relationship between output power and voltage differential (V_1⃝V_2). When the voltage difference reduces, the maximum output power drops to zero, according to the data.

A voltage differential between the converter output and the battery voltage can still be achieved by running the converter in boost mode and changing the duty cycle. Continuous power transfer is made possible in this way, even when $V = V$.

D. ZVS Condition Analysis

The switch can accomplish ZVS with the right control mechanism, according to the research. In order to give a thorough examination, the switch pair Q1 and Q2 is used as an example here. The waveforms of the gate signal, inductor voltage, and inductor current are displayed in Fig. 9 for the purpose of analysing ZVS. Specifically, the inductor current is split into four equal halves according to the gate signal's deadtime. Figure 10 shows the operating mode that corresponds to the ta, tb, tc, and td values in Figure 9. What follows is an examination of the data. In the first mode, shown in Figure 10(a), the inductor current is negative. Turn off switches Q1 and Q2. Diablo B1, which is connected in parallel with switch Q1, receives the current from the inductor when this condition is met.

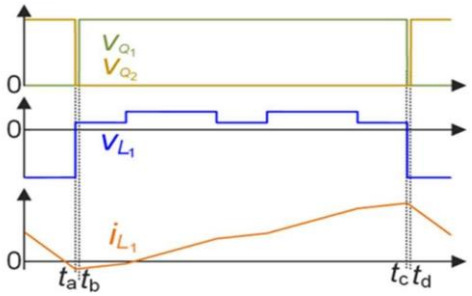


Figure 9: Waveforms of the gate signal, inductor
voltage, and inductor current utilised for ZVS analysis.

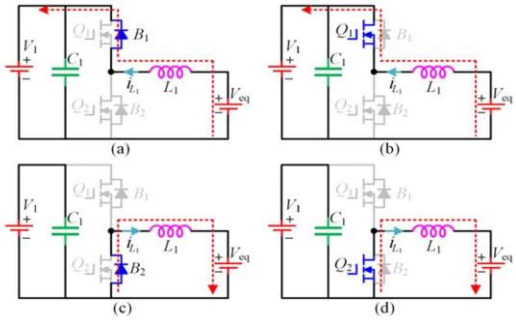


Figure 10 shows the ZVS in operation, with Veq representing the voltage source that is comparable to L1 and V2. (a) See Figure 9 for Mode 1: ta. (a) The second mode, shown in Figure 9, is tb. (c) In Figure 9 we have Mode 3: tc. (d) Mode 4: figure 9's td

In the second mode, shown in Figure 10(b), the inductor current is negative. Toggle Q1 is in the ON position. When this happens, current from the inductor goes into switch Q1. Switch Q1 can reach ZVS ON if its output parasitic capacitance can be entirely drained during deadtime. In the third mode, shown in Figure 10(c)], the inductor current is non-zero. Turn off switches Q1 and Q2. The current from

International Journal of
AI ELECTRICAL CIVIL AND MECHANICAL ENGINEERING
Peer Reviewed, Referred & Indexed Journal
ISSN: 3070-0434 www.zesterapublications.com Original Research Paper

the inductor is now flowing into the parallel-connected diode B2 through switch Q2. Level 4 (Fig. 10(d)): A current greater than zero flows through the inductor. You have
switched on Switch Q2. This causes electricity to flow into switch Q2 from the inductor. Switch Q2 can reach ZVS ON if its output parasitic capacitance can be entirely drained during deadtime. Achieving zero voltage suppression (ZVS) relies on completely discharging the output parasitic capacitance during deadtime. As can be shown in Figure 9, the output parasitic capacitance energy must be entirely discharged for switches Q2 if the maximum inductor current value is greater than a certain positive value. Likewise, with Q1 switches, the inductor current must not be less than a specific negative number. The circumstances for ZVS can be stated as the inductor current does not fluctuate much during dead time.

$$-i \quad , \quad , \quad t > 2V\ C$$

which gives

$$i \quad , \quad , \quad < -\frac{2V\ C}{t} \qquad (18)$$

and

$$i \quad , \quad , \quad t > 2V\ C$$

which gives

$$i \quad , \quad , \quad > \frac{2V\ C}{t} \qquad (19)$$

where

C is the output parasitic capacitance of the switch, and
t is the dead-time.

To achieve ZVS, the minimum inductor current is modified, which also changes the maximum inductor current. The new expression for the maximum inductor current is

$$i_{L1,max} = i_{L1,min,zvs} + \frac{(V_1 - V_2)(2V_1 + 3V_2)}{6V_1 L_1 f_s} \qquad (20)$$

Under this condition, the output power becomes

$$P_o = 3V_2 i_{L1,min,zvs} + \frac{V_2(V_1 - V_2)(2V_1 + 3V_2)}{4V_1 L_1 f_s} \qquad (21)$$

Equation (21) differs from equation (16) in that it incorporates an extra DC bias factor, which modifies the output power versus switching frequency curve somewhat. The general connection between switching frequency and output power is, nevertheless, unaltered.
The formula for determining inductance is

$$L = \frac{V \cdot t}{\Delta I} \qquad (22)$$

III PROPOSED CONTROL METHOD

When designing the control method, the switching frequency and output voltage ripple need to be considered. They are analysed in detail as follows.

A. Determination of Switching Frequency

The output voltage ripple is determined by the ripple current of the equivalent inductor L . The relationship between the inductor ripple current and the output voltage ripple can be expressed as

$$\frac{1}{2} \cdot \frac{1}{2} \Delta i \quad \cdot \frac{1}{2} \cdot \frac{1}{3} T_s = \Delta V\ C$$

which gives

$$\Delta V = \frac{\Delta i}{24C\ f} \qquad (23)$$

The ripple current of inductor $L$is defined as

$$\Delta i \quad = i \quad , \quad - i \quad , \qquad (24)$$

According to Fig. 6, the minimum and maximum currents of inductor L can be written as

$$i \quad , \quad = i \quad (t) + i \quad (t) + i \quad (t)$$

$$i \quad , \quad = i \quad (t) + i \quad (t) + i \quad (t) \qquad (25)$$

By analyzing the inductor current waveforms shown in Fig. 6, the expressions of the currents at instants t and t can be obtained. (For simplicity, the detailed derivation process is omitted here.)

Substituting (23), (24), and (25) into the derived current expressions yields the output voltage ripple as

$$\Delta V = \frac{(3V - 2V)(V - V)}{48C\ f\ L\ V} \qquad (26)$$

International Journal of
AI ELECTRICAL CIVIL AND MECHANICAL ENGINEERING
Peer Reviewed, Referred & Indexed Journal
ISSN: 3070-0434 www.zesterapublications.com Original Research Paper

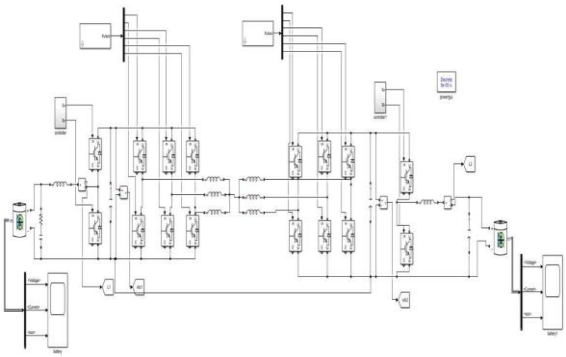
A number of variables, including V_1, V_2, C_2, L_1, and the switching frequency f_s, are shown to affect the output voltage ripple in equation (26).

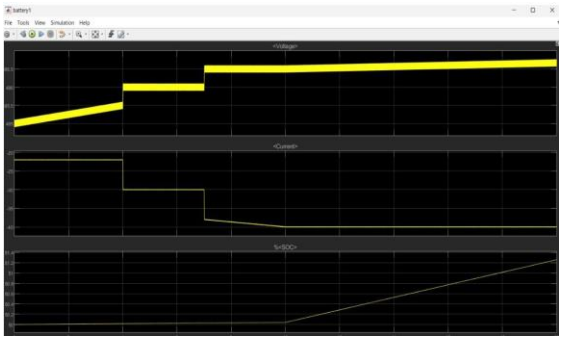
The values of V_1, V_2, C_2, and L_1 are known for vehicle-to-vehicle (V2V) energy transfer applications. Consequently, the output voltage ripple is precisely proportional to the switching frequency.

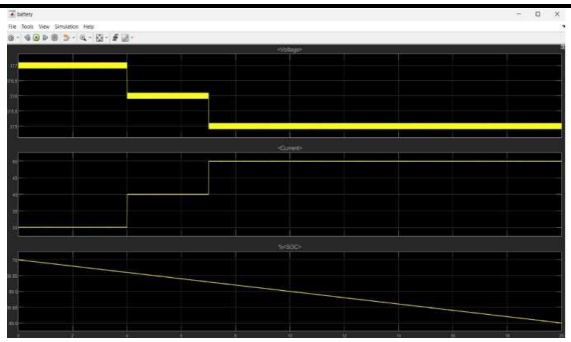
Also, when the switching frequency goes down, the power output goes up. The minimal switching frequency that may be considered while developing the control strategy is thus dependent on the required permissible output voltage ripple.

Hence, by establishing a tolerable limit for the output voltage ripple and computing the appropriate minimum switching frequency using (26), the maximum transferrable power may be ascertained.

IV Simulation Results







V CONCLUSION

In order to implement a V2V power transmission application, this article utilises the motor inverter and motor winding of electric vehicles to construct a topology. There is a thorough examination of the voltage gain, zero torque EV motor state, and ZVS switch condition. A technique for variable frequency control using ZVS is provided based on these study results. By reducing the switching frequency to several hundred Hz at high transmission power, the suggested control approaches were able to decrease switching loss and motor stator core loss, as shown in simulation results of 150 kW. To demonstrate the suggested method's superiority, it is compared to the current state of-the-art procedures using a table. The suggested approach was lastly validated with a 1.5 kW trial.

References

[1] N. Kumar, B. Singh, and B. K. Panigrahi, "Voltage sensorless based model predictive control with battery management system: For solar PV powered on-board EV charging," IEEE Transactions on Transportation Electrification, vol. 9, no. 2, pp. 2583–2592, Nov. 2023.

[2] F. Zinnari, S. Strada, M. Tanelli, S. Formentin, and S. M. Savaresi, "Electrification potential of fuel-based vehicles and optimal placing of charging infrastructure: A large-scale vehicle-telematics approach," IEEE Transactions on Transportation Electrification, vol. 8, no. 1, pp. 466–479, Mar. 2022.

[3] S. Hosseini and A. Yassine, "A novel V2V charging scheme to optimize cost and alleviate range anxiety," in Proc. IEEE Electrical Power and Energy Conf. (EPEC), Dec. 2022, pp. 354–359.

[4] A. Shafiqurrahman, V. Khadkikar, and A. K. Rathore, "Electric vehicle-to-vehicle (V2V) power transfer: Electrical and communication developments," IEEE Transactions on
Transportation Electrification, vol. 10, no. 3, pp. 6258–6284, Sep. 2024.

International Journal of
AI ELECTRICAL CIVIL AND MECHANICAL ENGINEERING
Peer Reviewed, Referred & Indexed Journal
ISSN: 3070-0434 www.zesterapublications.com Original Research Paper

[5] S. Dutta, A. K. Rathore, and V. Khadkikar, "Single-phase bridgeless converter for on-board EV charger with flexible charging capabilities," IEEE Journal of Emerging and Selected Topics in Industrial Electronics, vol. 4, no. 4, pp. 1170–1180, Oct. 2023.

[6] E. Ucer et al., "A flexible V2V charger as a new layer of vehiclegrid integration framework," in Proc. IEEE Transportation Electrification Conf. and Expo (ITEC), Jun. 2019, pp. 1–7.

[7] L. Li, G. Xu, W. Xiong, D. Liu, and M. Su, "An optimized DPS control for dual-active-bridge converters to secure full-load-range ZVS with low current stress," IEEE Transactions on Transportation Electrification, vol. 8, no. 1, pp. 1389–1400, Mar. 2022.

[8] P. He and A. Khaligh, "Comprehensive analyses and comparison of 1 kW isolated DC–DC converters for bidirectional EV charging systems," IEEE Transactions on Transportation Electrification, vol.
3, no. 1, pp. 147–156, Mar. 2017.

[9] M. O. Badawy et al., "Design and implementation of a 75-kW mobile charging system for electric vehicles," IEEE Transactions on Industry Applications, vol. 52, no. 1, pp. 369–377, Jan. 2016.

[10] M. Nasr et al., "SiC based on-board EV power-hub with highefficiency DC transfer mode through AC port for vehicle-to-vehicle charging," in Proc. IEEE Applied Power Electronics Conf. and Expo (APEC), Mar. 2018, pp. 3398–3404.

[11] S. Taghizadeh et al., "A multifunctional single-phase EV onboard charger with a new V2V charging assistance capability," IEEE Access, vol. 8, pp. 116812–116823, 2020.

[12] T. J. C. Sousa et al., "Comparative analysis of vehicle-to-vehicle (V2V) power transfer configurations without additional power converters," in Proc. IEEE International Conf. on Compatibility, Power Electronics and Power Engineering, Jul. 2020, pp. 88–93.

[13] S. Taghizadeh et al., "Design and implementation of an advanced V2V power transfer operation using communications," in Proc. IEEE International Conf. on Environment and Electrical Engineering, Jun. 2018, pp. 1–6.

[14] T. J. C. Sousa et al., "New perspectives for vehicle-to-vehicle (V2V) power transfer," in Proc. IEEE Industrial Electronics Society Conf., Oct. 2018, pp. 5183–5188.

[15] S. K. Vempalli and K. Deepa, "A novel V2V charging method addressing the last mile connectivity," in Proc. IEEE Power
Electronics, Drives and Energy Systems Conf., Dec. 2018, pp. 1